Geophysics Open-File Report No. 23
Geoscience Department
New Mexico Tech
Socorro, NM 87801

THREE DIMENSIONAL CRUSTAL VELOCITY MODEL BENEATH THE SOCORRO, NEW MEXICO AREA FROM INVERSION OF RELATIVE TRAVEL-TIME RESIDUALS

by

Saihay Tang

Submitted in partial
fulfillment
of
Geophysics 590
and the
Master's Degree Program
at
New Mexico Institute
of
Mining and Technology

March, 1978

The research described in this paper was sponsored in part by the New Mexico Energy Institute - New Mexico State University (EI-176-032 and EI-177-083).

Table of Contents

Acknowledgements

I would like to thank the members of my committee, Dr. A. Budding, Dr. A. Sanford and particularly my advisor, Dr. J. Schlue, for his patience and his great help throughout this study.

Abstract

Relative travel-time residuals of P-waves from mining explosions and teleseismic events obtained by Yousef (1977) and Fischer (1977) respectively vary over a range of about 1.05 seconds in the Socorro, New Mexico area. The residuals, caused by seismic heterogeneities, may be indicators of the presence of magma bodies in the crust.

An inversion of these seismic data using a method similar to that of Aki, Christoffersson, and Husebye (1977) gives a three-dimensional crustal model (to a depth of 37 km) of the P velocity beneath the stations. Minor low-velocities appear at shallow depths (within 9 km below the surface) of the model, roughly in the area where shallow magma bodies are proposed (Shuleski, 1976). No significant low-velocities are obtained deeper than 9 km, although high-velocity zones show up in the lower crust (18 - 37 km). It is hard to explain, at least at this stage, whether the high-velocity zones are caused by some compensating effects with the adjacent low-velocity zones, or whether they indicate thinning of the crust, or some other reasons.

Chapter 1 Introduction

Studies of microearthquake activity in the Socorro, New Mexico area have revealed the existence of an extensive magma body in the crust. Two sharp arrivals on microearthquake records at about 2.5 and 5 seconds after the direct S phase have been interpreted as the S_zP and S_zS reflections from a crustal discontinuity approximately 18 km below the surface (Sanford and Long, 1965). Further investigation concluded that the discontinuity was very sharp. From studies of observed S_zP and S_zS amplitude ratios, this sharp discontinuity is best explained as a boundary between matter in a solid and molten state, most probably the top of an extensive magma body (Sanford and others, 1973). The minimum depth to the body was found to be 17.8 km beneath the Socorro-Lemitar Mountains, increasing to 20 km at the edges (Rinehart, 1976). The southern boundary of the body is at 34°N approximately, and it extends at least 60 km north of Socorro. The minimum total area covered is estimated to be 1700 km^2. Analysis of some observations suggests that the body is quite thin, ie., sill-like in shape, although its thickness is still unknown.

Three types of observations suggest there exist shallow magma bodies that may be fed by the large, deeper magma chamber:

(1) SV waves are absent or very small for some microearthquakes in the Socorro area. Although some of these observations can be explained by earthquake mechanisms, others are apparently due to screening by materials with low rigidity (Shuleski, 1976).

(2) Anomalously high Poisson's ratio(0.26) in the upper crustal rocks for Socorro area in comparison with the value(0.22) obtained in the northern part of the Rio Grande Rift (Caravella, 1976).

(3) Spatial distribution of microearthquakes

Rinehart (1976) found that most of the microearthquakes in the Socorro area occur in swarms; moreover, hypocenters are diffusely distributed within the Rio Grande Rift with pockets of activity occurring 3 km north of Socorro, 7 km southwest of Socorro and 11 km southwest of Socorro. Approximately 60 % of the hypocenters have a depth of between 6 to 9 km and the deepest ones do not exceed 14 km. Since it is believed that spatial distribution of swarms are associated with magmatic activities, the spatial distribution of swarms suggests that there may be intrusions of magma taking place at relatively shallow depths.

Other geological and geophysical features relevant to the proposed magma bodies in this area are: (1) a high rate of surface uplift, with a maximum average rate of 6.1 mm per year, approximately 23 km north of Socorro (Reilinger and Oliver, 1976), and (2) anomalously high heat flow (Reiter and Smith, 1977).

In addition to the above analyses, new studies which are independent from what has been done are expected to shed some light on the problem. The primary purpose of this study is to use relative P-wave delay times from mining explosions and teleseisms to investigate the three-dimensional P-wave velocity structure beneath the Socorro area. Since the seismic velocity of the rock might decrease as much as 50 % when the rock undergoes a phase change from the solid to the molten state (Murase and McBirney, 1973), the regions where the magma bodies are proposed to be are thus expected to have a velocity lower than that of the average value of the surrounding region. Hence any low-velocity zone found from an analysis

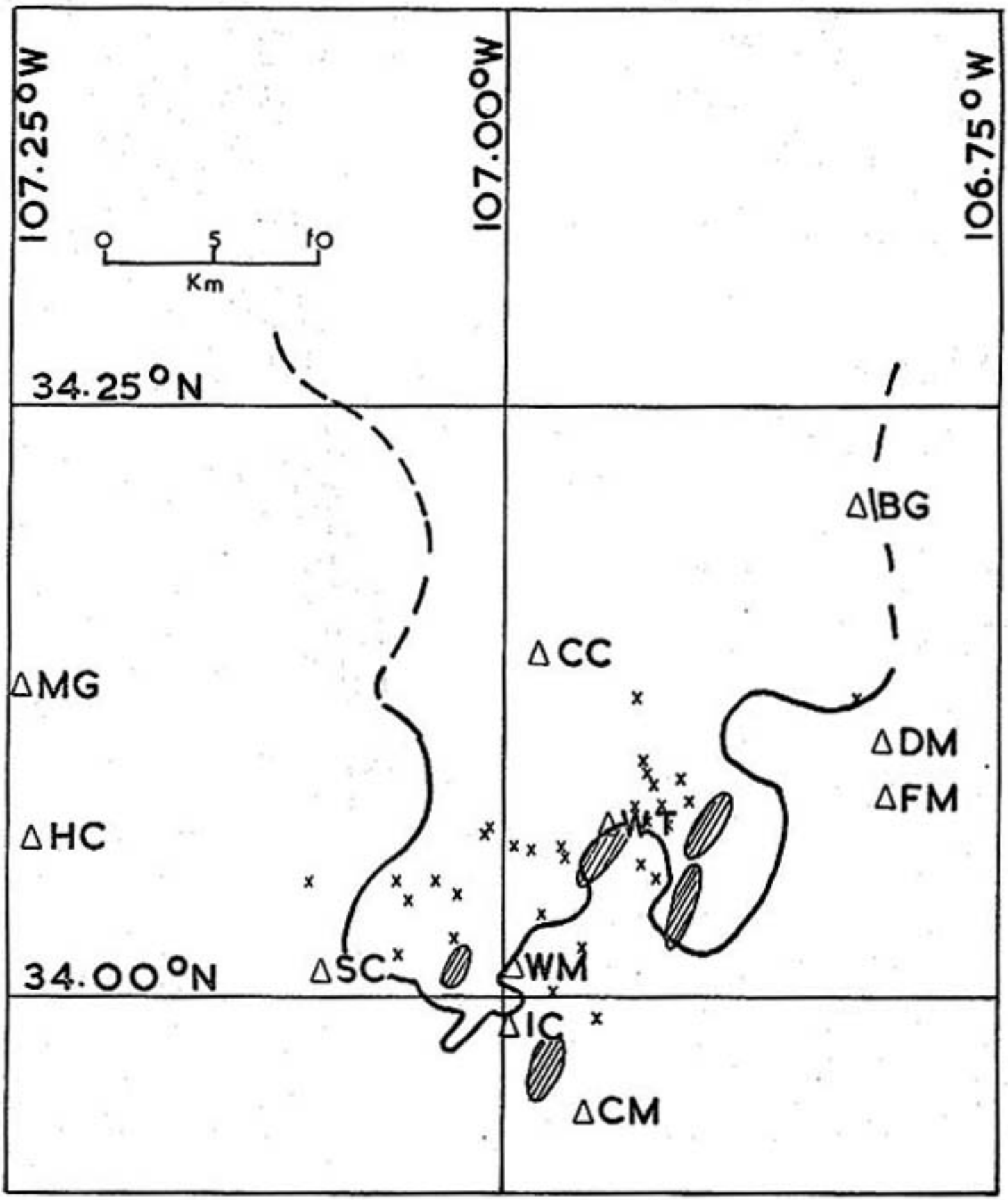

Figure 1. Boundary of extensive magma layer at depths of 18 to 20 km and location of shallow magma bodies with respect to location of earthquake swarms (from Rinehart, 1976).

may be an indicator of the presence of magma bodies. The data to be modeled are the relative delay times of the P-wave arrivals at various stations with respect to a base station. Two types of seismic events, mining explosions and teleseisms, are used in this study.

(1) Mining explosions: by using the daily explosions at Santa Rita, Tyrone (New Mexico) and Morenci (Arizona), Yousef (1977) constructed relative travel-time residual maps. These maps showed that the residuals became more negative (ie., advanced relative to the base station) to the southwest with the contours having a NW-SE orientation. This suggests the possibility of the existence of some low-velocity material near the base station such that the waves which travel to the base station are slowed relative to the waves which travel to the other stations.

(2) Teleseisms: Fischer (1977) used 46 teleseismic events to obtain residual maps showing a result directly opposite that of Yousef's. His work showed relative delays to the south and southwest of the base station.

Chapter 2 Formulation of the Problem

For a more detailed treatment of the generalized linear inverse method, readers may consult Backus and Gilbert (1968), Jackson (1972) and Braile (1973). Aki and others (1977) have introduced a method of inverting P-wave travel-time residuals to obtain three-dimensional seismic velocity models of the crust and upper mantle. This technique has been shown to be a useful tool for the study of lateral variations in crust and upper mantle structures. A similar procedure is employed in this study to investigate the P-wave structure of the crust beneath the Socorro area.

The travel-time residual at a particular station with respect to the base station is defined as the difference between the first arrivals at that station and the base, i.e.,

$$\Delta t_i = t_i - t_{base}$$

where t_i is the P-phase arrival athe i-th station,

t_{base} is the P-phase arrival at the base station, and

Δt_i is the travel-time residual at the i-th station.

Two ensembles of data, obtained from mining explosions (Yousef, 1977) and teleseisms (Fischer, 1977) are used in this study (see Appendix II). There are 139 observations, of which 112 are from teleseismic events. Station WT is taken as the reference station in both cases.

The initial model, consists of four homogeneous layers, of which the three upper layers each have a constant thickness of 9 km. The bottom layer is 10 km thick, for a total crustal thickness of 37 km (Sanford and Toppozada, 1976). Each layer is divided into sixteen blocks of uniform size bounded by lines of latitude and longitude; each has a NS

dimension of 22 km and an EW extension of 28 km, approximately (figure 2).

The region outside of this 'model zone' is referred to as the 'standard earth' and is assumed known. Ray paths traveling from distant foci to adjacent stations are considered to have taken the same path through the 'standard earth'. The residuals (Δt_i), if any, are regarded as arising directly from inhomogeneities in the 'model zone'. Hence, no exact knowledge about origin times and hypocentral parameters of the events is required. This is one main advantage of Aki's method, in that we are free from errors which might arise in the estimation of those parameters.

The theoretical travel time from a hypocenter to a station is

$$t_i^{th} = \sum_{j=1}^{n} \frac{A_{ij}}{V_j} + t_o$$

where j is the index for the parameters (compartments),

A_{ij} is the length of the ray path from event i through compartment j,

V_j is the P-wave velocity associated with compartment j, and

t_o is the travel time in the 'standard earth'.

(See Appendix I for the computation of A_{ij}).

The theoretical travel-time residual at a particular station with respect to WT is then

$$\begin{aligned} \Delta t_i^{th} &= t_i^{th} - t_{i,WT}^{th} \\ &= \left(\sum_{j=1}^{n} \frac{A_{ij}}{V_j} + t_o \right) - \left(\sum_{j=1}^{n} \frac{A_{ij}^{WT}}{V_j} + t_o \right) \\ &= \sum_{j=1}^{n} \left(A_{ij} - A_{ij}^{WT} \right) / V_j \end{aligned}$$

The superscript WT specifies the ray to station WT. It is sometimes convenient to use the slowness, which is defined as the reciprocal of the velocity, as a parameter instead of the velocity itself. Use of slownesses as parameters allows the problem to be linearized as follows:

The theoretical travel time residual appears in the form $(A_{ij} - A_{ij}^{wt})S_j$,

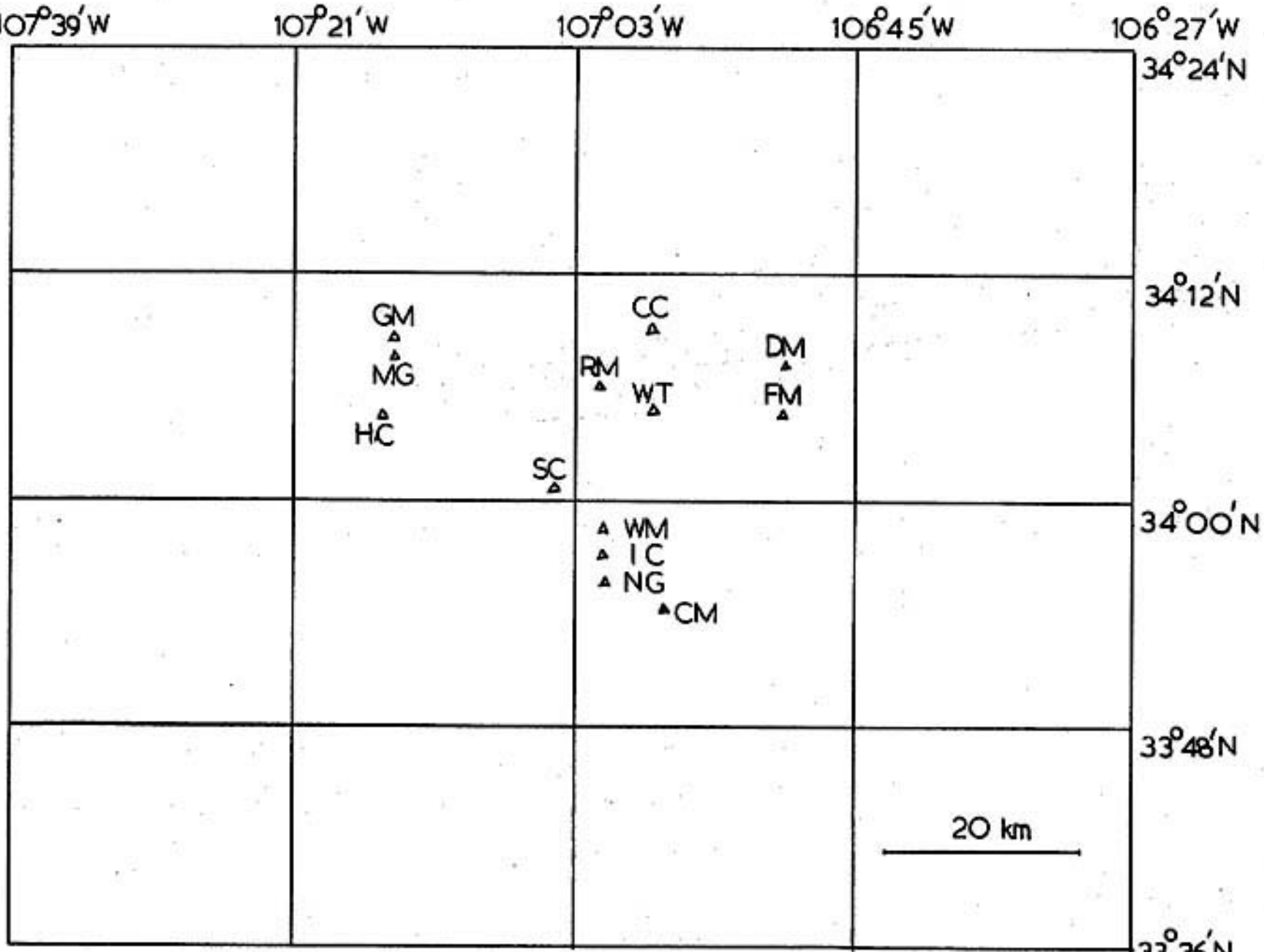

Figure 2. Boundaries of the model with locations of the 13 stations which recorded mining explosion and/or teleseismic arrivals used in this study.

where S_j is the slowness, $j = 1,2,\ldots,n$. After changing from velocities to slownesses, the time residual becomes a linear function of slownesses as the terms $(A_{ij} - A_{ij}^{wt})$ are constant under the assumption that no refraction occurs when a ray travels from one block to the other.

If we expand Δt_i^{th} by Taylor's Series, we obtain

$$\Delta t_i^{th}(\underline{S}) = \Delta t_i^{th}(\underline{S}^o) + \frac{\partial}{\partial S_j}\left[\sum_{j=1}^{n}(A_{ij} - A_{ij}^{wt})S_j\right]\Delta S_j$$

$$= \Delta t_i^{th}(\underline{S}^o) + (A_{ij} - A_{ij}^{wt})\Delta S_j , \qquad j = 1,2,\ldots,n$$

where the superscript o denotes the starting model. Higher order terms all vanish since Δt_i^{th} is a linear function. If we replace $\Delta t_i^{th}(\underline{S})$ by the observed time residual, namely Δt_i^{ob}, we have

$$\Delta t_i^{ob} = \Delta t_i^{th}(\underline{S}^o) + (A_{ij} - A_{ij}^{wt})\Delta S_j .$$

Defining

$$\delta t_i = \Delta t_i^{ob} - \Delta t_i^{th}(\underline{S}^o)$$

we have

$$\delta t_i = (A_{ij} - A_{ij}^{wt})\Delta S_j , \qquad \text{where } i = 1,2,\ldots,m \text{ and, } j = 1,2,\ldots,n$$

or in a more handy matrix form

$$\delta \underline{t} = \underline{A}\,\Delta \underline{S} \qquad \ldots\ldots \qquad (1)$$

where $\delta \underline{t}$ is an (m by 1) column vector,

$\underline{A}$ is an m by n constant matrix, and

$\underline{S}$ is an (n by 1) column vector.

Since we have more observations than parameters in this study (ie., $m > n$) the problem is overdetermined. Our main purpose is to find a perturbation vector, $\Delta \underline{S}$, such that when $\Delta \underline{S}$ is added to $\underline{S}^o$, $\delta \underline{t}$ will tend to a minimum. In general, we can solve (1) for $\Delta \underline{S}$ by finding a generalized inverse matrix of $\underline{A}$, using the principle of eigenvector decomposition (Jackson, 1972). Accordingly, $\underline{A}$ can be decomposed into

$$\underline{A} = \underline{U}\,\underline{\Lambda}\,\underline{V}^t \quad \ldots\ldots \quad (2),$$

where $\underline{U}$ is an m by n matrix whose columns are n eigenvectors of length m associated with the rows of matrix $\underline{A}$,

$\underline{\Lambda}$ is an n by n diagonal matrix containing the square roots of the eigenvalues of $\underline{A}\underline{A}^t$ ($\underline{A}^t$ is the transpose of $\underline{A}$),

$\underline{V}$ is an n by n matrix whose columns are n eigenvectors of n associated with the matrix $\underline{A}^t\underline{A}$.

A generalized inverse for $\underline{A}$ is given by Jackson (1972)

$$\underline{H} = \underline{V}\,\underline{\Lambda}^{-1}\,\underline{U}^t \quad \ldots\ldots \quad (3)$$

where $\underline{\Lambda}^{-1}$ is the inverse of $\underline{\Lambda}$. Thus from (1) we have,

$$\Delta\underline{s} = \underline{H}\,\delta\underline{t}$$

In order to have a well-defined generalized inverse $\underline{H}$ we have to eliminate the zero and near-zero eigenvalues in $\underline{\Lambda}$ as well as their associated eigenvectors. We then have $\underset{n\times m}{\underline{H}} = \underset{n\times p}{\underline{V}}\ \underset{p\times p}{\underline{\Lambda}^{-1}}\ \underset{p\times m}{\underline{U}^t}$ where p is the number of eigenvalues kept; p may also be considered to be the number of degrees of freedom in the problem.

We may weight the matrix $\underline{A}$ by the uncertainties in the observations to account for the effect of inaccurate data. A transformation of $\underline{A}$ is made, namely $\underline{A}' = \underline{C}\underline{A}$, where $\underline{C}$ is an m by m diagonal matrix whose elements are the reciprocals of the corresponding standard deviations of the observations. In addition, the same weighting is applied to the data vector,

$$\delta t_i' = \delta t_i / \delta_i \quad , \quad i = 1,2,\ldots,m$$

where δ_i is the corresponding diagonal element of $\underline{C}$.

With this weighting, an equation of exactly the same form as (1) is obtained and the same procedure as described above can be used to find $\Delta\underline{s}$; the

final model is given by $S_j = S_j^o + S_j$, $j = 1,2,\ldots,n$

A measure of the uniqueness of the solution can be found by the resolution operator $\underline{R}$, which is a matrix relating the 'true' parameters to the estimated parameters. $\underline{R}$ is an identity matrix if there exists only one solution. The resolution matrix is defined as

$$\underline{R} = \underline{H}\,\underline{A} = \underline{V}\,\underline{V}^t \quad \ldots\ldots \quad (4)$$

A measure of how much the resolution matrix differs from an identity matrix is given by

$$r_k = \sum_{i=1}^{n} \sum_{j=1}^{p} (V_{kj} V_{ij} - \delta_{ki})^2, \quad k = 1,2,\ldots,n$$

where V_{kj} is the element of matrix $\underline{V}$.

Low values of r_k (less than 0.5) indicate a delta-like character of the k-th row of the $\underline{R}$ matrix, implying the k-th parameter is a very localized average, whereas if r_k approaches 1.0, the resolving power of the data is very poor for that particular parameter.

The variance of the k-th parameter for statistically independent data is

$$\mathrm{var}(S_k) = \sum_{j=1}^{p} \left(\frac{V_{kj}}{\lambda_j}\right)^2 \quad \ldots\ldots \quad (5)$$

where λ_j is the diagonal element of the matrix.

Using (4) and (5) we can obtain an estimate of the variance and the r_k of each parameter as a function of p, the number of eigenvalues and eigenvectors used in constructing $\underline{H}$. The degrees of freedom can then be determined by making some 'trade-off' balance between r_k and $\mathrm{var}(s_k)$. The choice of p is made by considering both $\mathrm{var}(s_k)$ and r_k; if p is decreased, the variance will be diminished at the expense of degrading the resolution of the parameter.

The scalar R, defined as

$$R = \left[\frac{1}{m} \sum_{i=1}^{m} \left(\frac{\Delta t_i^{obs} - \Delta t_i^{th,f}}{\sigma_i} \right)^2 \right]^{1/2}$$

where $\Delta t_i^{th,f}$ is the theoretical time residual obtained from the final model, is a gross estimate of the 'quality' of the solution. If R is much greater than 1, it implies that the model is too crude to fit the data or the errors in the data may be too small whereas when R is much less than 1, it indicates that a more detailed a model has been used than can be justified by the data or that the errors in the data overestimated. If R approximates unity, it indicates that an optimum solution has been obtained.

In some respects, it is convenient to work with slowness as the parameters. However, our primary interest is in velocities, thus transformation from slownesses to velocities is necessary. As $V = 1/S$, then $\Delta V \approx -1/S^2 \Delta S$ so $V_i^f = V_i^o + \Delta V_i = (S_i^o - \Delta S_i)/(S_i^o)^2$, $i = 1,2,\ldots,n$ where o and f stand for initial and final model respectively.

Similarly, the relation $\text{var}(s_k) = \sum_{j=1}^{p} (v_{kj}/\lambda_j)^2$, $k = 1,2,\ldots,n$ gives the variances associated with slownesses while an expression associated with velocities is needed.

The standard deviation σ_s is the square root of variance. Consider

$$(S + \sigma_s)^{-1} \approx S^{-1}(1 \pm \sigma_s/S), \quad \text{if} \quad \sigma_s \ll S$$

$$\text{Since } V = S^{-1}, \quad S^{-1}(1 \pm \sigma_s/S) \simeq V(1 \pm V\sigma_s),$$

$$\text{so} \quad (S + \sigma_s)^{-1} \approx V \pm V^2\sigma_s$$

Thus an uncertainty σ_s in slowness introduces a corresponding uncertainty σ_v equal to σ_s/S^2 in the velocity.

Chapter 3 Results of Inversion

Table 1 shows the initial model used for the crust beneath the Socorro area. The P-wave velocities adopted are based upon information from Sanford and Toppozada (1976).

layer	thickness (km)	P-wave velocity (km/sec)	lateral block size (km)	
			NS	SW
1	9	5.80	22	28
2	9	5.80	22	28
3	9	6.50	22	28
4	10	6.50	22	28

Table 1. Initial model parameters

(1) Teleseismic and mining explosion data

The first inversion attempts sought to obtain a four-layer model using both teleseismic and mining explosion data (139 residuals). The final model which contains 36 blocks with unknown P velocity appears in figure 3. Velocities greater than one standard deviation from the starting values are considered anomalous and are denoted by asterisks in the map.

In layer 1 (0 - 9 km), a low-velocity block that coincides roughly with the position of the five shallow magma bodies as proposed by Shuleski (1976) appears in the southeast. In this model, however, the low-velocity zone extends to the south of latitude 34°N, while Shuleski (1976) placed them somewhat northward. If this low-velocity area does reflect the existence of molten material, we may wish to estimate its dimension. If we assume a decrease of 50 % in the P-wave velocity in molten rocks (Murase and McBirney, 1973), we may

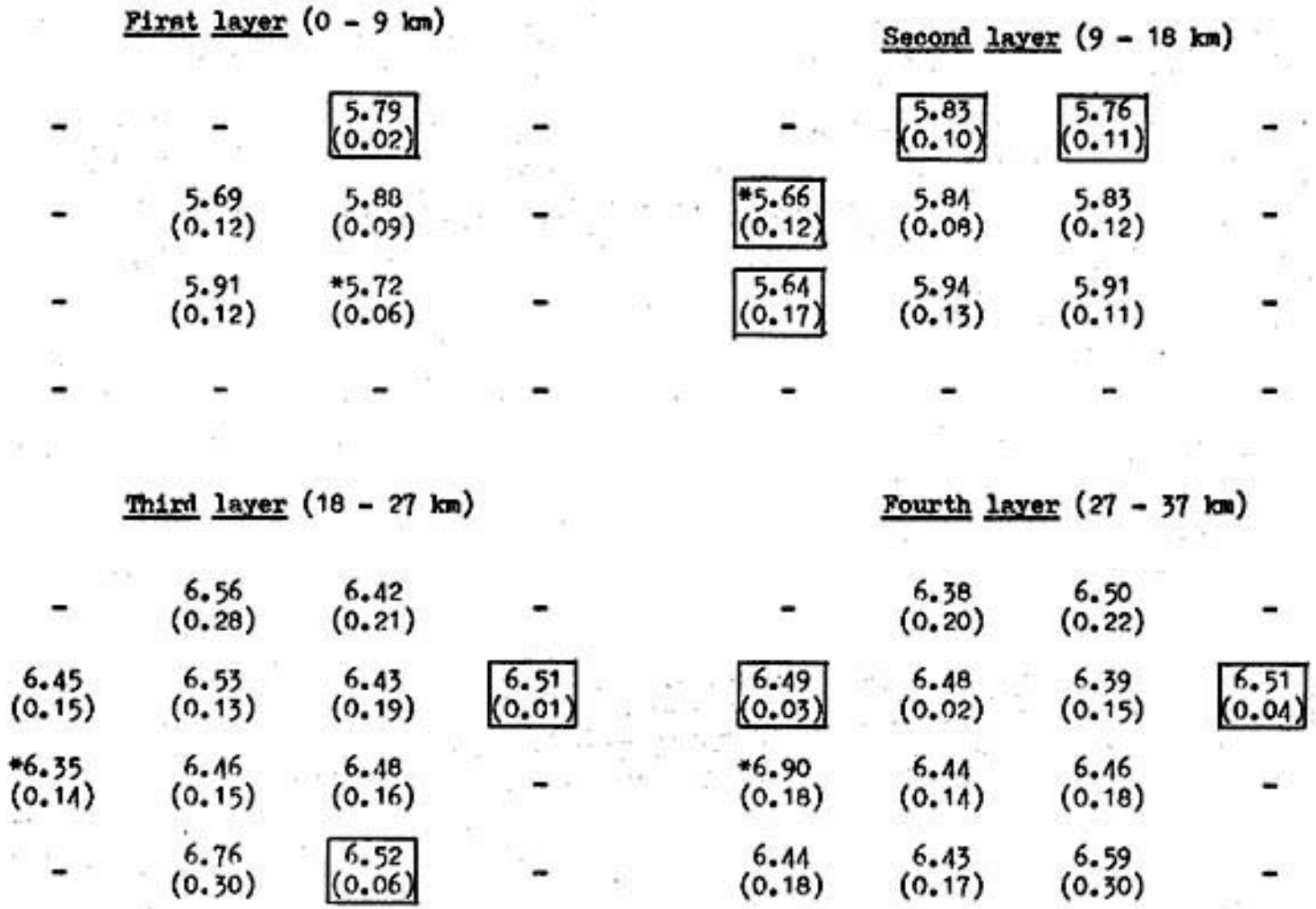

Figure 3. Inverse solution for a 4-layer model by using both teleseismic and mining explosion data. The numbers show the P-wave velocity in km/sec where the associated standard deviations are bracketed. Velocity anomalies are denoted by asterisks and blocks poorly resolved are enclosed in squares.

conclude that the 1.4 % decrease in P-wave velocity of the final model is equivalent to the presence of a magma layer of 0.11 km in thickness. The above assumption of a 50 % decrease will be used hereafter.

In layer 2 (9 - 18 km), half of the parameters are poorly resolved with corresponding resolving kernels ranging from 0.16 to 0.44. The physical implication of a resolution matrix is: if a particular diagonal element is close to unity (ie., delta-like in that row of the resolution matrix), then the corresponding parameter is said to be compactly resolved. In the other words, the effect is quite localized. However, if the diagonal element is small and with broad sidelobes, the associated parameter is said to be resolved as a linear combination of adjacent parameters. We illustrate these diagrammatically in figures 4 and 5. The shaded area in the figures represents velocity anomaly. In figure 4, parameter 1 may be resolved uniquely while in figure 5, the diagonal elements of the resolving kernels corresponding to parameters 1 and 2 may have broader sidelobes.

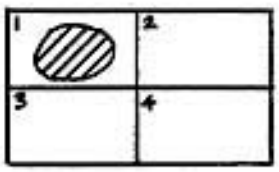

Fig. 4

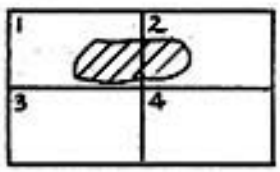

Fig. 5

Referring to the discussion of layer 2, among the ill-resolved parameters, a low-velocity anomaly shows up in the western portion of the model. Large negative sidelobes in its resolving kernel suggest that this low-velocity zone may not be contained in the actual model; only a combination effect with neighboring blocks.

The proposed extensive magma body at 18 km, if any, is the main interest of this study and is expected to appear in the northwestern area of the third layer (18 - 27 km). However, these parameters are all within one standard deviation of the initial average velocity. At the same time their associated uncertainties are generally larger than those of the upper two layers. It is possible that the existence of the magma body may be masked by these relatively large uncertainties. If we adopt a primitive estimate of the thickness of the magma body by Sanford (1977), i.e., 1 km, and use our previous assumption, we expect the blocks in this area could have velocities of 6.0 km/sec or lower. Hence, it is quite obvious that such an anomaly cannot be hidden by the indicated uncertainties. If we believe the existence of a magma body at 18 km, it could be masked by the present range of errors if its thickness is less than 0.6 km and a 40 % decrease in P-wave velocity is assumed.

A low-velocity block appears in southwestern portion of the model which overlies an anomalously high-velocity section in the fourth layer (27 - 37 km). This low-velocity zone is about 2 % lower than the average velocity of the layer, with a standard deviation which almost approximates this difference. In contrast, the underlying block can be regarded as having an anomalously high velocity, since its final velocity is more than two standard deviations from the average. Large values in the corresponding resolving kernels show that each of these two blocks is quite well-resolved and thus, this low-high velocity combination may be real and probably is not the result of velocity-balancing between adjacent blocks.

The scalar number R, which is an indicator of how well the solution

fits the data in a gross sense, equals 2.21 for this model, implying that the model is somewhat crude for the data.

(2) Teleseismic data only

Figure 6 shows the derived model when the teleseismic data are used alone. The original 36 parameters are reduced to 28 as some of the blocks have not been sampled. The final model shows that all of velocities lie within one standard deviation of the initial velocities. In other words, no anomalies are indicated.

As we examine the blocks in the third layer where the large magma pocket is proposed to be, we find that the associated uncertainties are larger than those of the previous case. However, we can still waive the possibility of existence of any magma layer thicker than 0.6 km following the same line of argument as before. The scalar number R has become smaller (equal to 1.64) for this case, which implies that the use of the teleseismic data alone provides a better fit than does use of the teleseismic and mining explosion data. However, this result is more likely caused by the larger uncertainties associated with the teleseismic data (Table 7, Appendix II) rather than by other cause.

Since homogeneous layers are indicated by the teleseismic data, the anomalies found in the first study are most likely from the mining explosion data. It is thus advisable to invert the mining explosion events alone even though the data available are few. In any case, we still have 24 parameters for 27 observations, making the problem over-determined.

First layer (0 - 9 km)

-	-	5.80 (0.03)	-	-
-	5.84 (0.22)	5.80 (0.15)	-	-
-	5.76 (0.20)	5.80 (0.13)	-	-
-	-	-	-	-

Second layer (9 - 18 km)

-	5.80 (0.09)	5.80 (0.12)	-
-	5.76 (0.25)	5.80 (0.20)	-
-	5.83 (0.24)	5.81 (0.17)	-
-	-	-	-

Third layer (18 - 27 km)

-	6.51 (0.35)	6.51 (0.31)	-	-
-	6.49 (0.23)	6.50 (0.21)	6.50 (0.25)	-
-	6.52 (0.27)	6.48 (0.22)	-	-
-	-	6.50 (0.07)	-	-

Fourth layer (27 - 37 km)

-	6.50 (0.22)	6.49 (0.36)	-
-	6.50 (0.19)	6.50 (0.18)	6.49 (0.68)
-	6.56 (0.33)	6.50 (0.19)	-
-	6.46 (0.33)	6.50 (0.33)	-

Figure 6. Inverse solution for a 4-layer model by using teleseismic events only. See figure 3 for explanation of symbols.

(3) Mining explosion data only

The result of the inversion is shown in figure 7. Unlike the results obtained by using teleseismic events alone, velocity anomalies in layer 1, 3 and 4 are resolved in this study. In layer 1, a 95 % confident level low-velocity zone is found located to the west of a high-velocity zone at the northern part of the model. The relatively large values of the corresponding diagonal elements of the resolution matrix do not suggest any combination between these two parameters or between others. If the low-velocity zone is really caused by the existence of magma body, then, using our previous assumptions, this may be corresponding to a magma body with a total thickness of approximately 0.8 km. However, it is most unlikely to have sill-shaped magma bodies of such large size at this shallow depth. If the magma body is dike-like, then, with the assumption that the average angle of incidence is 25°, the width of the dike is estimated to be 0.3 km (for a 50 % reduction in velocity).

The low-velocity zone in layer 3 is located to the west of the major area where the 18 km magma body is proposed to be. This low-velocity zone is quite well-resolved, whereas its adjacent block is somewhat model-dependent. The corresponding off-diagonal element of the resolving kernel indicates that there exists some combination effects between them. This low-velocity anomaly may reflect the possible presence of a very thin magma layer of about 0.2 km in thickness, which is certainly too slight an effect to be resolved with these data. Such a magma body could be easily masked by the uncertainties.

An anomalously high-velocity zone (at the 95 % confidence level)

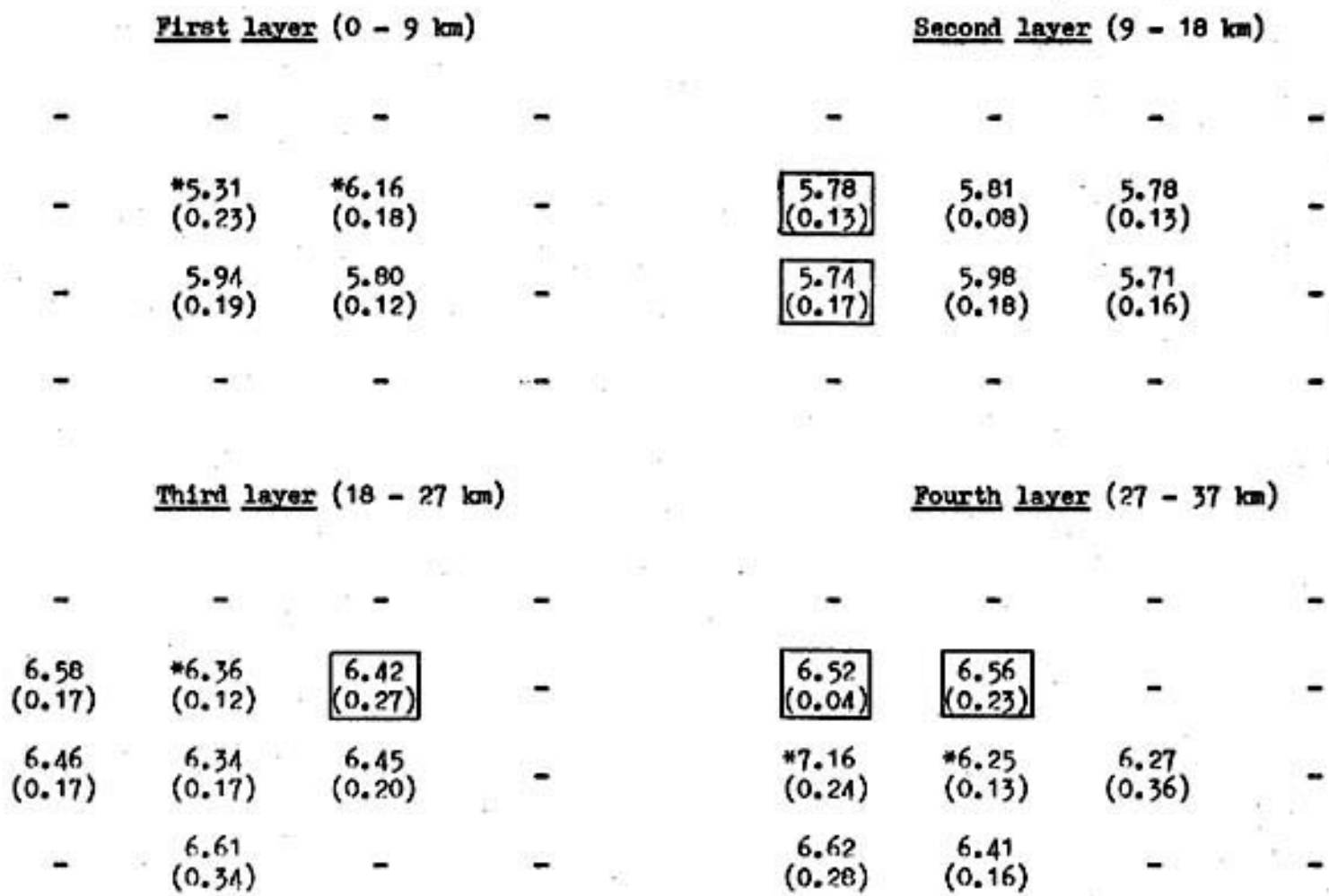

Figure 7. Inverse solution for a 4-layer model by using mining explosion data only. See figure 3 for explanation of symbols.

again shows up at the same position as found previously. To the east of it is a low-velocity zone. Analysis of the resolution matrix $\underline{R}$ indicates that both the high and low velocity zones are not uniquely resolved, but are resolved only in combination with a poorly-resolved block to the north. Thus, this high velocity-low velocity feature may be explained by some kind of compensation effect between each other. This may also be the case for the anomalies shown in the first layer. Another physical possibility is that the high-velocity block may indicate a thinning of the crust in this area. Once again, if the low-velocity zone is interpreted as a result of presence of molten material the block with the final average velocity of 6.25 km/sec may contain a magma layer of 0.4 km thickness.

The number R equals to 4.04 in this case, showing that the gross fit for the data set is the poorest among the three studies. The relatively small uncertainties in the observations are probably the reason.

Chapter 4 Discussion

A study of the results of our inversions shows that none of the final model fits the data very well ($R > 1$). This is especially true for those inversions which used only data from the mining explosions. It may be possible to obtain models which fit the data better by using more unknowns in the inversion. However, increasing only the unknowns will also increase the size of the uncertainties of these unknowns, so there is no guarantee that we can obtain better resolution of the unknowns. On the other hand, the geometry of the model is also a determining factor. Hence, it may be helpful to consider the distribution of seismic stations carefully before any future investigation.

As a first approach to the problem, it is quite natural to start with a model of relatively simple geometry as was done for this study. Thus, we set up a model comprised of blocks of uniform sizes. As a result, all the stations are concentrated on three blocks (see figure 2), since the stations are not evenly distributed throughout the model zone. The problem is that if a 'field' station and the base station are both sitting upon the same block, it is very likely that the rays will have more or less identical paths. If this is the case, the theoretical time residuals will always vanish, no matter how the parameters are being varied. As a result, the observational data can never be well-fitted by the theoretical model. For improvement, it is suggested that the blocks be constructed so that the stations could be located on top of as many different blocks as possible. However, the total number of parameters in the model is constrained by the capacity of the Tech computer. Moreover, it is also advisable not to have blocks with horizontal dimension less than 1 km. A large number of small

blocks may be geometrical ideal; the result, however, would probably be degraded resolution (large indicated uncertainties and/or poorly-resolved blocks).

Another factor that contributes significantly to the unsatisfactory resolution of the velocities found in this study is the relatively large uncertainties in the observed data. In this investigation, the majority of the data are from the ensemble of teleseismic events (112 observations out of 139). However, their associated standard deviations are relatively large in comparison with the observed time residuals. 60 % of the observed time residuals are less than their estimated uncertainties. As a result, the inversion using only teleseismic data obtained a solution which indicated that all the layers are essentially homogeneous. In the mixed ensemble of teleseismic and mining explosion data, 53 % of the residuals are less than their estimated uncertainties. The velocity anomalies delineated all arise from the mining data because the errors in their readings are relatively small. However, since the seismic rays from the mining explosions are all coming from south of the model zone, not much information can be obtained for the area north of Socorro. It is also hazardous to use mining data alone because the narrow coverage of azimuth may bias the final model. Better results may be expected if higher-quality teleseismic data (say, with errors less than 0.1 sec.) are obtainable.

Chapter 5 Conclusion

No velocity anomalies are indicated in the final model obtained from teleseismic data alone. If the mixed ensemble of teleseismic and mining explosion data is used, a shallow (0 - 9 km) low-velocity block located somewhat south of the positions of the five shallow magma bodies proposed by Shuleski (1976) is obtained; this velocity anomaly of 5.72 $\pm$ 0.06 km/sec may indicate the presence of a magma layer in the upper crust of 100 meters in thickness (assuming a 50 % drop in the P-wave velocity in the magma). When mining explosion data are used alone, a shallow (0 - 9 km) high-velocity block adjoining a low-velocity block is found at a location north of the low-velocity zone mentioned in the above case. As these two blocks are compactly resolved, there is the suggestion that this feature is not the result of some combination of effects, but is, in fact, real. If the low-velocity anomaly of 5.31 $\pm$ 0.23 km/sec is really caused by molten material, this may correspond to a sill-like magma body of 0.8 km in thickness, or a dike-like magma body of 0.3 km width. However, we do not expect to have thick magma layers at this shallow depth (0 - 9 km).

In layer 3 (18 - 27 km), the layer where an extensive magma chamber has been proposed, relatively large uncertainties for the final model may mask any low-velocity effect. We estimate that a magma layer, if any, could be as large as 600 meters in thickness (assuming a 50 % P-wave velocity drop) and still not be resolved because of the large uncertainties.

A high-velocity block is obtained at the 95 % confidence level in the bottom layer (27 - 37 km) in the southwest corner of the final model. A study of its resolving kernels shows that this block is quite compactly

resolved. It is hard to explain, however, whether the apparent high velocity is caused by high-velocity material, by crustal thinning or by some other possibility.

I conclude that this study has shown no evidence for a massive 18-km deep magma body, although such evidence could be hidden with the indicated uncertainties. Some indication of both a shallow (0 - 9 km) and a deep (27 - 37 km) magma body has been obtained. A high-velocity zone obtained in the bottom layer may be best explained by crustal thinning rather than by postulating high-velocity material. More data are needed, especially higher-quality teleseismic data from a variety of azimuths, before this technique can provide the resolution necessary to resolve anomalies at the scale derived here, much less to resolve anomalies to any finer scale.

Appendix I Computation of Length of Ray Path in the 'Model Zone'

As the planar boundary of the blocks are defined by longitudes and latitudes, distances from each station to the boundaries can be easily found provided that the locations of the stations are known (Richter, 1958, App. XII). Without loss of generality, we can illustrate the procedure for computation of the ray length in the 'model zone' by taking the following case as an example:

$L = 37 \times \tan i$ (in km)

where i is the angle of incidence

$l_1 = d_1/\cos(2\pi - \theta)$

$l_2 = d_2/\sin(2\pi - \theta)$

$l_3 = L - l_1 - l_2$

where θ is the azimuthal angle

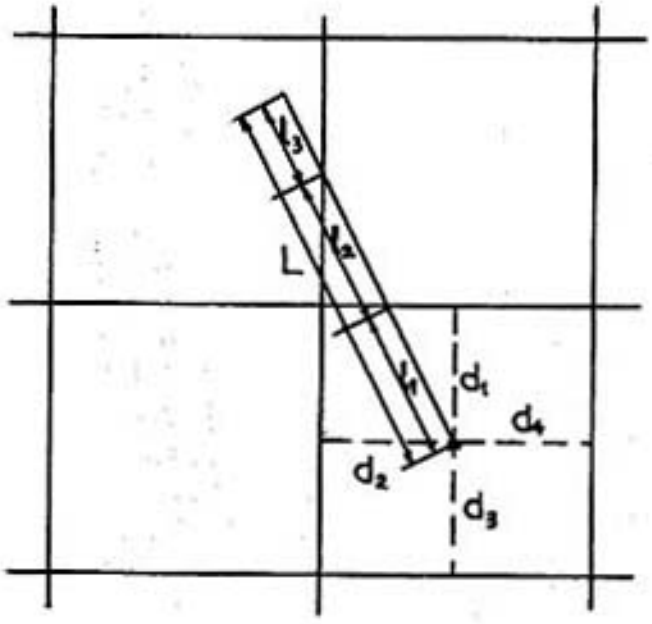

Plane view showing the station and ray path

It has been assumed that there is no refraction during transmission from one block to another; in other words, the ray paths are straight line segments rather than broken lines.

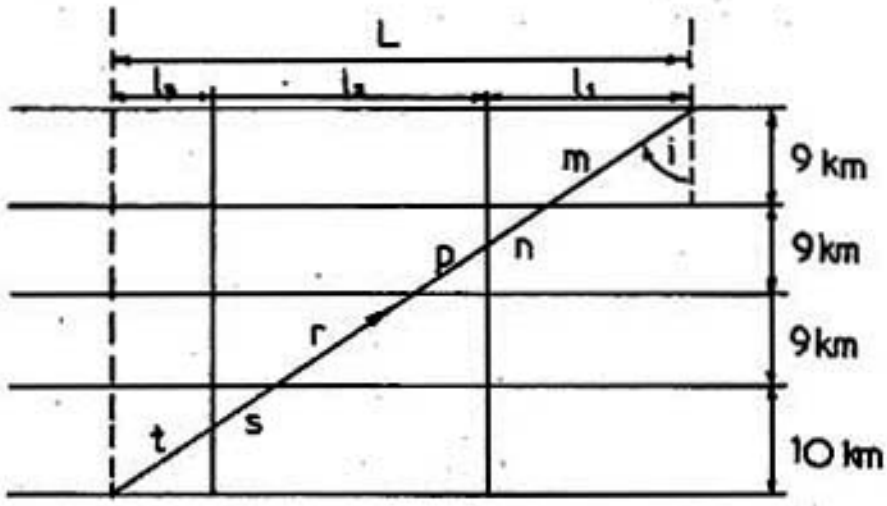

Diagram showing the ray path through the blocks

m, n, p, r, s and t are integers identifying distinct blocks. A_{jk} is the length of a ray path in a particular block, where the first index j specifies the observation and k is the index for the block.

$$A_{jm} = 9/\cos i$$

$$A_{jn} = (l_1 - 9 \tan i)/\sin i$$

$$A_{jp} = 9/\cos i - (l_1 - 9 \tan i)/\sin i$$

$$A_{jr} = 9/\cos i$$

$$A_{js} = 10/\cos i - l_3/\sin i$$

and $$A_{jt} = l_3/\sin i.$$

$A_{jk} = 0$ for blocks which have no ray segment.

Appendix II Miscellaneous Tables

Table 2. Locations of Recording Stations

Station	Latitude	Longitude
CC	34.144	106.981
CM	33.950	106.958
DM	34.108	106.808
FM	34.083	106.805
GM	34.145	107.235
HC	34.066	107.236
IC	33.987	106.997
MG	34.131	107.243
NG	33.965	106.993
RM	34.081	107.007
SC	34.010	107.089
WM	34.012	106.993
WT	34.072	106.946

Table 3. Locations of Santa Rita, Tyrone and Morenci

	Latitude	Longitude
SR	32.797	108.058
TR	32.645	108.373
MR	33.063	109.335

Table 4. Azimuthal angles of recording stations with respect to Santa Rita (SR), Tyrone (TR) and Morenci(MR).

Station	Azimuthal angles w.r.t.		
	SR	TR	MR
CC	214°	218°	242°
CM	219°	223°	247°
DM	219°	222°	245°
FH	219°	223°	245°
GM	207°	213°	239°
HC	209°	214°	241°
IC	217°	221°	245°
NG	218°	222°	246°
SC	214°	218°	244°
WT	216°	226°	224°

Table 5. Station Corrections*

Both Mining explosion and teleseismic data obtained by Yousef (1977) and Fischer (1977) respectively has been modified by following station corrections before use in this study.

Station	Station corrections (sec)
CC	0.14
CM	0.16
DM	0.03
FM	0.00
GM	0.16
HC	0.27
IC	0.22
MG	0.16
NG	0.25
RM	0.35
SC	0.27
WM	0.28
WT	0.00

* Schlue, personal communication

Table 6. Time residuals and standard deviations from mining explosions (after Yousef, 1977).

Stations	Explosions	Residuals(sec)	Uncertainties(sec)
CC	SR	-0.14	0.06
CC	TR	-0.09	0.05
CC	MR	-0.11	0.05
CM	SR	-0.12	0.05
CM	TR	-0.22	0.05
CM	MR	-0.19	0.06
DM	SR	-0.03	0.05
DM	TR	-0.02	0.05
DM	MR	0.00	0.05
FM	SR	-0.04	0.05
FM	TR	0.03	0.05
FM	MR	0.02	0.05
GM	SR	-0.12	0.05
GM	TR	-0.14	0.05
GM	MR	-0.17	0.05
HC	SR	-0.37	0.05
HC	TR	-0.29	0.05
HC	MR	-0.33	0.05
IC	SR	-0.26	0.05
IC	TR	-0.21	0.05
IC	MR	-0.25	0.06
NG	SR	-0.33	0.05
NG	TR	-0.24	0.05
NG	MR	-0.24	0.05
SC	SR	-0.35	0.05
SC	TR	-0.28	0.05
SC	MR	-0.28	0.05

Table 7. Data from teleseismic events (after Fischer, 1977)

Date	Station	Angle of incidence	Azimuthal angle	Observed time residual (sec)	error (sec)
3/20/75	CC	24°	310°	-0.28	0.10
	FM			-0.05	0.12
4/16/75	CC	22°	21°	-0.13	0.06
	CM			-0.15	0.08
4/16/75	CC	28°	136°	-0.04	0.12
	CM			0.18	0.14
7/29/75	CC	38°	309°	-0.03	0.10
	CM			0.26	0.12
	FM			0.18	0.12
	SC			-0.32	0.09
8/1/75	CC	21°	321°	-0.13	0.10
	CM			-0.07	0.12
	FM			0.15	0.12
	SC			-0.14	0.09
8/6/75	CC	16°	318°	0.19	0.10
	CM			0.38	0.12
	FM			0.59	0.12
	SC			0.05	0.09
8/12/75	CC	16°	242°	-0.12	0.13
	CM			0.06	0.15
	FM			0.13	0.35
	SC			-0.01	0.13
8/15/75	CC	22°	318°	-0.16	0.10
	CM			-0.10	0.12
	SC			-0.22	0.09
9/16/75	CM	14°	305°	0.02	0.12
	HC			0.24	0.11
	MG			0.05	0.22
	HG			0.08	0.10

Date	Station	Angle of incidence	Azimuthal angle	Observed time residual(sec)	error (sec)
10/28/75	CC	20°	143°	-0.19	0.12
	CM			-0.11	0.14
	SC			-0.16	0.10
10/29/75	CC	38°	157°	-0.13	0.12
	CM			0.01	0.14
	SC			-0.25	0.10
11/4/75	CC	22°	318°	-0.13	0.10
	CM			-0.10	0.12
	SC			-0.05	0.09
11/5/75	CM	26°	128°	-0.02	0.14
	SC			-0.05	0.10
1/20/76	CM	16°	239°	0.00	0.15
	DM			0.01	0.13
2/3/76	CC	14°	240°	-0.19	0.13
	DM			-0.18	0.13
	SC			-0.34	0.13
2/3/76	CC	16°	242°	-0.03	0.13
	CM			-0.07	0.15
	DM			0.16	0.13
	SC			-0.25	0.13
2/5/76	CC	20°	141°	0.11	0.12
	DM			0.13	0.22
	SC			-0.05	0.10
2/6/76	CC	15°	245°	-0.10	0.13
	CM			-0.01	0.15
	DM			-0.05	0.13
2/18/76	CC	23°	312°	-0.16	0.10
	CM			0.00	0.12
	IC			-0.07	0.35
	SC			-0.06	0.09
	WM			-0.05	0.35

Date	Station	Angle of incidence	Azimuthal angle	Observed time residual(sec)	error (sec)
2/19/76	CC	36°	146°	0.16	0.12
	CM			-0.01	0.14
	IC			-0.11	0.18
	SC			-0.10	0.10
	WM			-0.04	0.22
3/24/76	CM	15°	235°	-0.12	0.15
	DM			-0.27	0.13
	IC			-0.26	0.17
4/13/76	CC	40°	173°	-0.05	0.12
	IC			0.01	0.18
	SC			0.09	0.10
6/18/76	GM	15°	238°	0.40	0.25
	NG			-0.06	0.35
	RM			0.09	0.26
	SC			-0.10	0.13
	WM			0.15	0.35
7/1/76	GM	26°	101°	-0.15	0.35
	HC			-0.04	0.25
	NG			-0.41	0.25
	RM			-0.03	0.26
	SC			-0.01	0.10
7/15/76	HC	26°	100°	-0.17	0.25
	NG			-0.37	0.25
	RM			-0.33	0.26
	SC			-0.43	0.10
7/29/76	GM	15°	343°	-0.01	0.12
	HC			0.18	0.11
	NG			0.02	0.10
	SC			-0.07	0.09
8/4/76	GM	14°	308°	0.02	0.12
	HC			0.20	0.11
	NG			0.05	0.10
	SC			-0.06	0.09

Date	Station	Angle of incidence	Azimuthal angle	Observed time residual(sec)	Error (sec)
8/10/76	HC	26°	135°	0.08	0.25
	NG			0.07	0.25
	SC			-0.16	0.10
8/12/76	GN	17°	319°	0.10	0.12
	HC			-0.07	0.11
	NG			-0.16	0.10
8/20/76	GN	18°	314°	0.06	0.12
	HC			0.64	0.11
	NG			-0.07	0.10
	SC			-0.19	0.09
8/20/76	GN	20°	141°	0.21	0.35
	HC			0.60	0.25
	NG			-0.07	0.25
	SC			-0.04	0.10
1/21/77	CC	15°	245°	-0.23	0.13
	GN			-0.20	0.15
	DN			-0.16	0.13
	GN			-0.09	0.25
	SC			-0.21	0.13

Bibliography

Aki, K., A. Christoffersson and E. S. Husebye (1977). Determination of the three-dimensional seismic structure of the lithosphere, Jour. Geophy. Research 82, 277 - 296.

Backus, G. E. and J. F. Gilbert (1968). The resolving power of gross earth data, Geophy. Jour. Royal astr. Soc. 16, 169 - 205.

Braile, L. W. (1973). Inversion of crustal seismic refraction and reflection data, Jour. Geophy. Research 78, 7738 - 7744.

Caravella, F. J. (1976). A study of Poisson's ratio in the upper crust of the Socorro, New Mexico area, M.S. Independent Study, Geoscience Dept., New Mexico Inst. Mining and Tech.

Fischer, J. A. (1977). The use of relative travel time residuals of P phases from teleseismic events to study the crust in the Socorro, New Mexico area, M.S. Independent Study, Geoscience Dept., New Mexico Inst. Mining and Tech.

Jackson, D. D. (1972). Interpretation of inaccurate, insufficient and inconsistent data, Geophy. Jour. Royal astr. Soc. 28, 97 - 109.

Murase, T. and A. R. McBirney (1973). Properties of some common igneous rocks and their melts at high temperatures, Geol. Soc. Amer. Bull. 84, 3563 - 3592.

Reilinger, R. and J. E. Oliver (1976). Modern uplift associated with a proposed magma body in the vicinity of Socorro, N.M., Geology 4, 583 - 586.

Reiter, M. and R. Smith (1977). Subsurface temperature data in the Socorro Peak KGRA, New Mexico, Geothermal Energy Magazine 5, 37 - 41.

Rinehart, E. J. (1976). The use of microearthquake to map an extensive magma body in the Socorro, New Mexico area, M.S. Independent Study, Geoscience Dept., New Mexico Inst. Mining and Tech.

Sanford, A. R. and L. T. Long (1965). Microearthquake crustal reflections, Bull. Seismol. Soc. Amer. 55, 579 - 586.

Sanford, A. R. and J. Oliver(1977). Comparison of microearthquake and COCORP studies of magma bodies beneath the Rio Grande Rift in the vicinity of Socorro, New Mexico, Text of paper presented to the Joint General Assemblies of the International Associations of (1) Seismology and Physics of the Earth's Interior and (2) Volcanology and Chemistry of the Earth's Interior in Durham, England.

Sanford, A. R. and T. R. Toppozada (1976). Crustal structure in central New Mexico interpreted from the Gasbuggy explosion, Bull. Seism. Soc. Amer. 66, 877 - 886.

Sanford, A. R., O. Alptekin, and T. R. Toppozada (1973). Use of reflection phases on microearthquake seismograms to map an unusual discontinuity beneath the Rio Grande Rift, Bull. Seism. Soc. Amer. 63, 2021 - 2034.

Shuleski, P. J. (1976). Seismic fault motion and SV wave screening by shallow magma bodies in the vicinity of Socorro, New Mexico, M.S. Independent Study, Geoscience Dept., New Mexico Inst. Mining and Tech.

Yousef, A. A. (1977). A study of time residuals in the Socorro area for P_n arrivals from mining explosions at Santa Rita, Tyrone, New Mexico, and Morenci, Arizona, M.S. Independent Study, Geoscience Dept., New Mexico Inst. Mining and Tech.